The International Journal of Engineering and Science (IJES)
|| Volume || 13 || Issue || 3 || Pages || PP 01-08 || 2024 ||
ISSN (e): 2319 – 1813 ISSN (p): 2319 – 1805

Experimental Investigation to Analysis the Impact Damage of Un-Peened and Peened Of Aa7075-T6 Using Water Jet Peening Processes.

JAMAL-DEEN KUKURAH[1], VITUS MWINTERIBO TABIE[2], ANTHONY AKAYETI[1], JOSEPH SEKYI-ANSAH[3],JAMES KWASI QUAISIE[4], ABDUL-HAMID MOHAMMED[4],PHILIP YAMBA[1], BISMARK ADDAI[5].

[1]*Faculty of Engineering (Mechanical Engineering Department, Tamale Technical University, Tamale, Ghana*
[2]*Faculty of Engineering (Mechanical Engineering Dept.), Hila Liman Technical University, Wa, 00233, Ghana*
[3]*Mechanical Engineering Department, Takoradi Technical University, Takoradi, Ghana*
[4]*Faculty of Engineering (Welding & Fabrication Department, Tamale Technical University, Tamale, Ghana*
[5]*Materials Engineering Department, Sunyani Technical University, Sunyani, Ghana*
[*]*Corresponding author*

----------***ABSTRACT***----------
This article presents the impact damage of un-peened and peened of AA7075-T6 specimen using water jet peening processes. The mechanical properties on residual stress, micro hardness, fatigue test and fracture surface morphology of an AA7075-T6 were investigated. In this experiment, an electro-hydraulic servo control test machine, Vickers micro-hardness tester,scanning electronic microscope and optical microscope were utilized to observe the residual stress, micro hardness, fatigue test and fracture surface morphology of an AA7075-T6 under different incident pressures. The results indicated that the residual stress, micro hardness, fatigue test and fracture surface morphology of the AA7075-T6 material increases as the incident pressures increases.

Keywords: *impact damage; un-peened; water jet peening; micro hardness; surface morphology.*

Date of Submission: 01-03-2024 Date of acceptance: 08-03-2024

I. Introduction

Thermal fatigue cracking has been observed in numerous industrial components that are subjected to cyclic thermal loading. This kind of failure is most common in high-temperature applications where the materials are regularly subjected to temperature variations, like engines and boilers in power plants. Variations in temperature can produce residual strains that, because of recurrent expansion and shrinkage, inevitably lead to thermal fatigue damage. There are two main stages to the process of thermal fatigue failure. First comes the creation of cracks, also known as the basic stage. These fissures then have the ability to spread, indicating the secondary stage [1]. Thermal stresses are created when cracks first appear and are susceptible to growing and spreading due to temperature variations. The fatigue life of a component is the number of cycles beyond which it will ultimately fail. This phrase refers to tiredness in both its initial and spreading stages [2]. The intricate damage mechanism of thermal fatigue cracking is dependent on a number of variables, such as component shape, stress conditions, and material properties [3]. Thus, by taking into account the operational loading circumstances and material parameters, the thermal fatigue crack propagation prediction can assist engineers in proposing an acceptable component designation and properly predicting the lifetime [4]. The mechanical characteristics, fatigue lifespan, and resistance to corrosion of metallic materials can all be adversely impacted by surface imperfections [5]. Therefore, in order to reduce or completely eradicate any defects, the surface of metallic material must be treated with any necessary post-treatments [6]. There has been research into a few laser-based, mechanical, and chemical surface post-treatment techniques to enhance the fatigue characteristics of metallic materials. Salehnasab et al. [7]study examined the impact of a conventional shot peening treatment on the development of thermal fatigue cracks and solid solution alloy failure mechanisms. The findings show that, especially along the crack propagation path, shot peening causes compressive residual stress, which reduces the distribution of thermal stress. The simulated and experimental data for crack growth agreed well, as seen by the simulated fatigue life curve produced by ZENCRACK. The rate of thermal fatigue crack growth was significantly reduced by the addition of shot peening, and an increase was observed during the heating stage according to the simulated stress intensity factor analysis. As a result, throughout the heating-up procedure, the

thermal fatigue crack spread. According to SEM analysis, the shot peening post-treatment affects the start and spread of thermal fatigue cracks. Moreover, non-shot-peened specimens show trans-granular cracking, whereas shot-peened specimens show inter- and trans-granular cracking as their failure mode. The effects of shot peening, cavitation peening, and submerged laser peening on the enhancement of the fatigue strength of magnesium alloy AZ31 were compared by Soyama et al. [8]. The findings of their investigation suggested that in order to ascertain the appropriate coverage, the fatigue life at a constant bending load was investigated. For the SLP, CP, and SP specimens treated by each optimal condition, the fatigue strengths at N = 107 were found to be 56%, 18%, and 16% higher, respectively, than that of the non-peened (NP) specimen, which was 97 MPa. Work hardening and the addition of compressive residual stress were the two main components that allowed peening techniques to increase fatigue strength. A study on ultrasonic pulsed waterjet peening of commercially pure titanium was carried out by Siahpour et al. [9]. The applied traversal speed and stand-off distance as well as the observed surface roughness and residual stress were shown to be correlated in the experimental results. Moreover, it was demonstrated that UPWJ enhances the surface mechanical behavior with respect to both scratch hardness and Rockwell hardness (HRB). Increased stand-off distance and faster traverse speed led to a maximum of −391 MPa in induced compressive residual stress, while maintaining moderate levels of surface roughness (i.e., Ra <3 μm). This study illustrates the potential of UPWJ for surface modification of CP-Ti alloy while eliminating the possibility of surface contamination, which can be harmful in many applications, by comparing it with shot peening. There is also a brief discussion on the comparison of UWPJ used for peening Ti-6Al-4V (Grade 5). Yong and associates [10] Utilizing synchrotron X-ray diffraction, residual strain in Inconel 718 additively fabricated by laser shock peened is evaluated. Owing to the samples' layer-by-layer manufacturing, a periodic strain variation was observed. The peened sample did not show an increase in diffraction peak width in the near-surface regions. This contradicts published research using wrought laser shock-peened alloys and demonstrates decreased grain disturbance in additively produced peened samples. The results are relevant given the present drive to significantly boost the production efficiency of aero-engine components through the use of additive manufacturing. The effects of intermediate cerium salt conversion bath treatment and ultrasonic shot peening on the corrosion of magnesium-Y-zinc-based alloys in seawater were investigated by Ashok Kamde et al. [11]. The subsurface characteristics of the specimens subjected to XRD, FESEM, surface topography, and Vickers hardness analysis show that CePT coating prior to USP reduces surface roughness (R_a = 1.91–2.38 μm vs R_a = 2.58–2.76 μm) and increases microhardness (~142–149 $HV_{0.05}$ vs ~ 125–135 $HV_{0.05}$). Potentiodynamic polarization and electrochemical impedance spectroscopy show that for specimens subjected to USP + CePT treatment together, corrosion current decreased (I_{corr}~ 9.81–13.69 μA/cm^2 vs. ~ 23.82–26.22 μA/cm^2), coating (R_1), and polarization resistance (R_2) increased to ~ 1704–1907 Ω.cm^2 and ~ 1834–1902 Ω.cm^2, respectively, indicating superior corrosion resistance. Overall, by creating a ceramic coating that is interlocked with the surface and functions as a barrier between the metal/solution interface, an intermediate CePT prior to USP can successfully reduce corrosion pitting phenomena of WZ_{44} alloy in chlorinated solution. Si et al. [12]study examined how ultrasonic shot peening improved the surface-modified 2024T351 Al alloy's resistance to cavitation erosion. The results showed that the USP-ed sample's cavitation weight loss was greatly decreased when surface hardening and residual compressive stress worked together. After three hours of UCE treatment, the weight loss for the USP-ed 2024T351 Al alloy with an intensity of 0.101mmA was 54.2% lower than that of the untreated sample. Additionally, this study discovered that the cavitation resistance qualities may be lowered by the increased surface roughness that results from shot peening. However, surface polishing can prevent the deterioration. The findings suggest that USP is a promising physical strengthening technique that can greatly increase metals' resistance to cavitation erosion. A study titled "Notch fatigue life prediction of micro-shot peened 25CrMo4 alloy steel: A comparison between fracture mechanics and machine learning methods" was carried out by Li et al. Li et al. [13]. The findings demonstrate that, in comparison to unpeened specimens, the compressive residual stress (CRS) of shot-peened specimens increases their fatigue life. While the machine learning method's prediction nearly falls within the error band of ±1.5, the fracture mechanics method's prediction falls within the error band of ±2. The two most important variables influencing the HCF fatigue life are the stress level and notch size.

In this study water jet peening was used to investigate the mechanical properties on residual stress, micro hardness, fatigue test and fracture surface morphology of an AA7075-T6.

II. Materials And Methods

2.1 Materials

The material that has been used for this investigation is 7075-T6 grade aluminum alloy. Because of its excellent mechanical strength to weight ratio, the aluminum alloy AA7075-T6 is widely utilized in high-tech applications.The 7075-T6 grade aluminum alloy specimens were prepared with the dimensions shown in Figure 1. this is to do reconnoitre on the effect of water jet peening on the FCG rate on AA7075-T6. The positions of the water jet peening zone on AA7075-T6 were carefully marked by marking pen input to distinguish from

different zones treatment. In referenced from figure 1, the notched growth samples/specimens were prepared by Cutting specimens at stated dimensions by electro-discharge machined (EDM); with a Notched-growth depth direction of 3 mm by an angle of 900; Grinding and polishing samples with SiC paper at different grades of roughness; Cleaning samples in deionized water and saving in drying box and Eliminating machined surface residual stress of notches growth specimens by naturally aging treatment for a particular interval of time. Table 1 shows the chemical composition of the AA7075-T6 material.

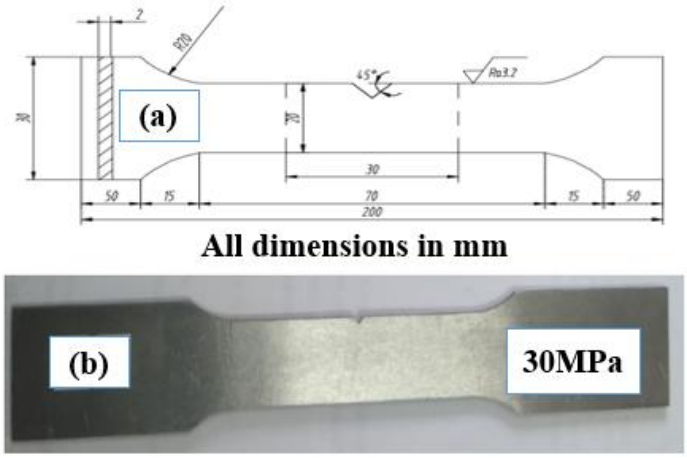

Figure 1. shown specimen of AA7075-T6: a) Dimension and b) photo

Table 1. AA7075-T6 workpiece chemical composition

AA7075-T6	Cr	Cu	Fe	Mg	Mn	Si	Ti	Zn	Al
	0.18	1.40	0.11	0.25	0.05	0.25	0.07	4.8	Bal.

2.2 Experimental setup

The Principles, experimental parameters of water jet peening and the properties of the materials used, setups of residual stress, Vickers hardness test, fatigue test and fracture morphologies observation. The experimental setup for fatigue, together with its initial fracture and ultimate rapture, are depicted in the samples in figure 2(a). Before the test, tap water is kept in a huge 2.5 m × 2 m × 1.5 m tank at a temperature of 25 ± 2 °C for at least 24 hours. A transparent water tank with a height of 800 mm and a square horizontal cross-sectional area of 400 mm × 400 mm is used for the tests. For flow visualization, acrylic resin was used to create the tank. The nozzle utilized in this experiment is depicted in Fig. 2(b), and it was made with an angular nozzle in mind to produce the cavitating jets' periodic behavior[14]. When the nozzle's throat diameter (d) is 1.5 mm, its throat length (L) is 12 mm, and its expansion angle (θ) is 30 °, the ideal size ratio is d:L = 1:8 [15]. It should be noted that the nozzle was 150 mm below the water's surface, and the plunger pump was used to force the flow through it in order to create the submerged cavitation jets in the high-pressure test cell. The nozzle's upstream and downstream pressures were measured using a pressure transducer. The pressures on this article are severe. The majority of the experiments were conducted at incident pressures of 15 MPa, 20 MPa, and 25 MPa, despite the plunger pump's maximum operating pressure of 35 MPa. The radial flow of material may be impeded by the 26 N blank holder force. The distance between the surface of the test specimen and the nozzle exit is known as the standoff distance S. The standoff distance S in this experiment was set at 110 mm. Within the cell, the metal foil was positioned perpendicular to the cavitating jets. 1O millimeters was the set axial distance (SL) between the jet axis and the micro-die cavity (the eccentricity SL was also 10 millimeters). It was found after multiple experiments (with incidence pressures ranging from 15 MPa to 25 MPa) that the developing feature was on the cavitation ring when the eccentricity SL was 10 mm. Five (5) minutes made up the test duration (t).

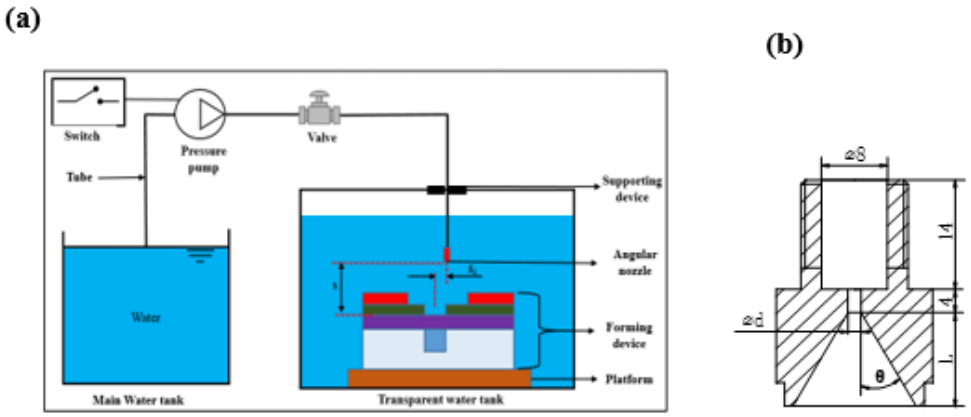

Figure 2(a) Experimental system of cavitating water jets shock micro-forming; (b) nozzle geometry diagram.

III. Results and discussion

3.1 Residual stress

Residual stress Related work on the surface over the central-hole which was performed under experimental results and distribution curve of the cross-correlation function with and without water jet peening were presented in Figure 3 samples peened 15 MPa, 20 MPa, and 25 MPa. The residual stress of untreated was 9 MPa and 15 MPa, 20 MPa, and 25 MPa, were 15 MPa, 17 MPa, and 24 MPa. The curve of cross-correlation of untreated material peak values 5.4a residual stress observed was 9 MPa in figure 3. The maximum residual stress in the one side shocked direction gave 24 MPa corresponding energy pulse but 1-4 peak value of 118 was increased to 740, 762 and 751. But residual stresses peak values in one-sided shocked was vice versa in figure 3.

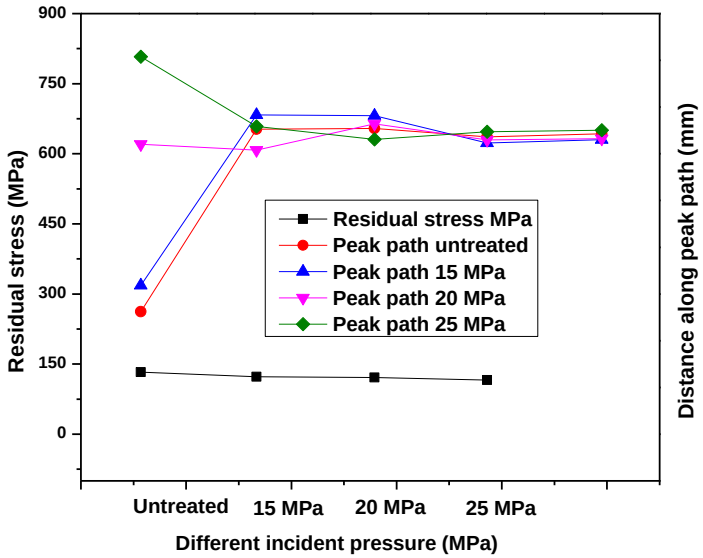

Figure 3 Residual stress and different incident pressures levels on samples

3.2 Microhardness

The microhardness profiles comparison for untreated and treated water jet peening samples is shown in figure 4 that untreated, (15 MPa, 20 MPa, and 25 MPa), gives a hardness percentage of 116.37%, 117.72%, 119.76%, 122.10% respectively. The microhardness of untreated material takes a constant value of approximately 116.35 % of HV along the parallel direction. The microhardness profiles for both water jet peening conditions are similar but gave different percentage levels. The maximum and minimum value obtained compared differences of 25 MPa and untreated was 10.94 % of HV then drop gradually to 0% of untreated material around a depth of 1.17 %. It is found Cleary that the untreated material presents a fixed micro-hardness in the parallel direction to roll, this can be credited to more compact and elongated. This shows that the hardness of the AA7075-T6 material increases as the incident pressure increases.

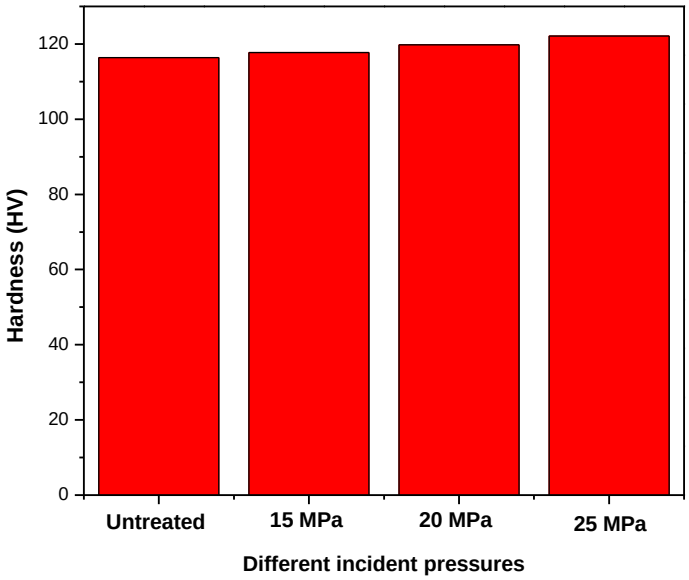

Figure 4. Performance of water jet peening energy levels and hardness test

However, the benefit of the water jet peening treatment is that it increases the hardness and eliminates anisotropy in the near-outward layer. Dhanasekaran[16], reported an increase in near-surface microhardness after water jet peening treatment in AA7075-T6. However, the increased in water jet peening energy of 15 MPa and 20 MPa micro hardness increase is lower than that found in the MPa worked. This fact could be ascribed to energy differences of spot size.

3.3 Fatigue test

From Figure 5 shown a fatigue life cycle to the failure of unpeened sample, 15 MPa, 20 MPa, and 25 MPa, resulted in 3418, 3593, 3893, 3994. The best improvement is given by water jet peening conditions. Again in both figures 5 and 6 that water jet peening condition lasted higher cycles and times to failure analogous to 1456 cycle difference in improvement with respect to untreated specimens of untreated (3418 cycles to failure) and 25 MPa (4874 cycles to failure). This shows that the failure increases as the incident pressure increases.

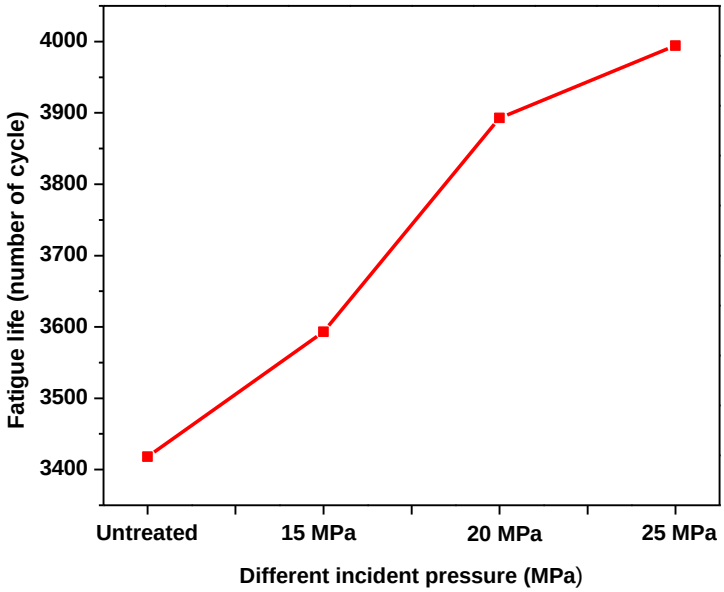

Figure 5. Fatigue life cycle of specimens subjected to different water jet peening processes

Again from figure 6 of time to failure of unpeened sample, 15 MPa, 20 MPa, and 25 MPa, also resulted in 1152, 1208, 1357, 1407 respectively While figure 6 water jet peening condition lasted 409 seconds difference in time to failure analogous to the improvement of 25 MPa (1407 seconds) and unpeened sample (1152 seconds). This shows that the failure increases as the incident pressure increases. Ge et al. [17]investigated the

swept line of fatigue life on 316 L stainless steel alloy. Contrary to the results displayed in the present AA7075-T6, these authors reported that improvement was observed when the swept line is parallel to the specimen longitudinal axis.

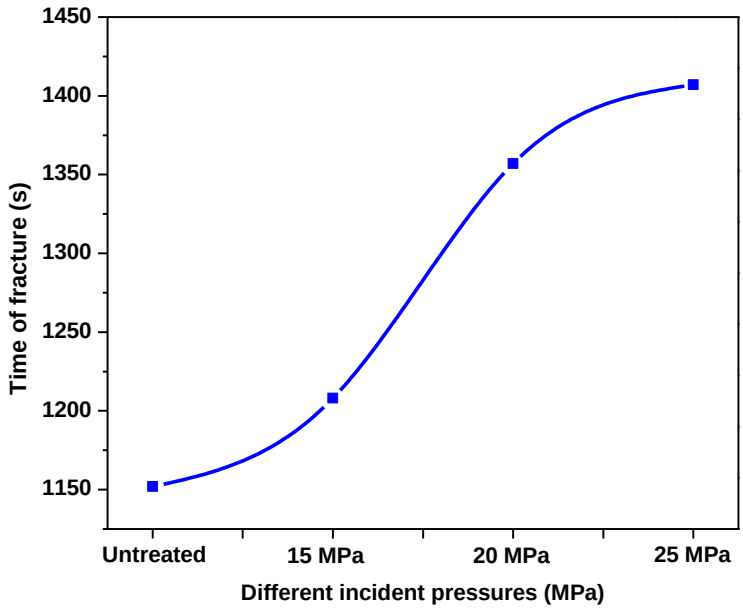

Figure 6. Different incident pressures of water jet peening and time of fracture

In this hold, a circumstance such as tensile stresses in the mid-thickness (due to the equilibrium of stress state) and residual stresses persuade at the sample boundaries are attributed to possess a high sway on the fatigue existence. Moreover, the water jet peening decorations should also be taken into account. The maximum outward layer hardness was secured with the spiral-type swept direction. Ge et al. [17] suggested a haphazard type swept marking, which realize a notable lessen the residual stresses anisotropy when compared to zig-zag swept design. In this work, it is revealed that the material's microstructural anisotropy engenders by rolling also affects the dispensation and accordingly convert the fatigue behavior. In AA7075-T6 microstructural features including chemical composition phases, phase distribution, grain size, and heat treatment influence crack initiation and growth. This test quota of plastic contortion controlled the load split between austenite and ferrite. Fatigue life is allied with the gradual gathering of plastic contortion in regions localized (crystalline defects), which, after several loading cycles gives rise to the crack incubation. The residual stresses persuade by water jet peening impede outmost force and lessen the strain magnitude in the territory close by outward layer. Similarly, the enlargement in hardness holds up the crack initiation in these vulnerable regions. This revealed both the presence of residual stresses and surface hardness results of AA7075-T6.

3.4 Fracture surface morphologies

The typical fracture morphologies of FCG region on AHSS DP 350/600 subjected to water jet peening are shown in figures from 7 to 10. It can be seen that fatigue crack region of the untreated and treated specimens initiated from the sharp-angled place along the notch edges in figure 7 untreated. b), and figures 8 to 10); 15 MPa, 20 MPa, and 25 MPa. It can be found that crack sources had been transferred from the top surface to the superficial layer along the depth direction. It is well known that the fatigue crack region location closely associates with the complex microstructures [18] especially, fatigue crack region location depends on the influence of crack tip grain. The slip-lines engender on the metal surface under cyclic loading, gradually mount up and form a fatigue slip striation. The fatigue crack is introduced on the bushiest blunder marking [19]. Associated with the non-gliding expanse, the harvest stress and hardening amount of material in the slithering region reduction, which varieties the ounces descending calmer. It can be contingent that fatigue crack finally pledges in the region with a high density of slid patterns. In fact, the energy of fatigue slid striations bring together in the dishonest credit of the water jet peening specimens, caused the fatigue crack region position calmer to provoke in the insincere film subsequently water jet peening. Moreover, water jet peening presented countless complexity of CRS on the preserved superficial, which can meaningfully decrease the plastic strain [20] on the portion shallow underneath fatigue freight [21]. The CRS improved the fatigue boundary of the reinforced deposit and induces fatigue cracks to recruit at the vulnerable area, where working stress is abundant slighter than that at the superficial. This can also elucidate the fact that the location of crack foundations is far

away from the top exteriors in the item "c" of both figures of 7(b) to (d) (15 MPa.; 20 MPa.; and 25 MPa.). This shows that as the incident pressure increases the surface morphology increases.

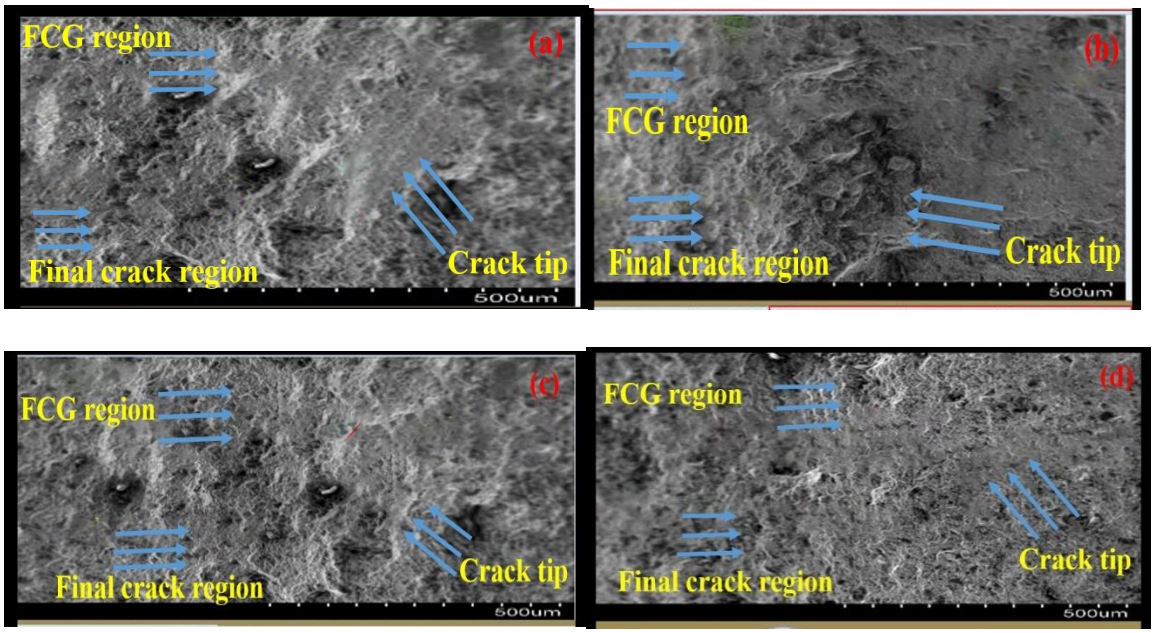

Figure 7. Morphologies of both FCG and final fracture region on untreated sample:
(a) untreated; (b) 15MPa; (c) 20 MPa; (d) 25 MPa.

However, the fatigue striation on a fracture surface is a very important character which aids to comprehend circumstances associated with the fracture, including the number of stress differences that fashioned the breakage. Moreover, patterns can advance a needle to regulate the directionality of fracture propagation. The FCG paths of specimens at the primary FCG period was initiate that adequately of fatigue striations positioned at the FCG period, and the spacing among the head-to-head patterns was unvarying. FCG path of unprocessed specimens was even, and the fatigue pattern arrangement was broader. However, the nonconformity happened to FCG pathway after water jet peening figures 5.14 to 5.16, and the fatigue pattern spacing developed lesser. In totalling, manifold shocked and energy raised of water jet peening upsurges the plastic distorting and eventually produces a tremendously high displacement density, which delays the crack circulation and decreases the FCG rate. It is healthy distinguish that the fatigue marking space is the estimate of FCG rate [274], so it can be decided that FCG degree reductions ceaselessly with the upsurge of water jet peening coverage area at the early stage. Final fracture morphologies clearly shown that the dimples morphologies at finial fracture stage of AA7075-T6 specimens subjected to water jet peening with different coverage of energy. The fracture phase offerings a static-loading and prompt distinguishing with numerous well-dispersed dimples and microporous-congregated topographies. It can also be seen from the figures 5.10 to5.16 that the dimples for the untreated specimens was equiaxial and well-distributed. However, the dimple size of the treated specimens apparently increased figures item of 5.14 to 5.16. As said earlier before, the grain rotation and the low angle boundaries of subgrains generated by water jet peening process lead to a high resistance to the glide of crystal surface throughout stumpy set fatigue. The water jet peening constrains the joining of microporesand thus upsurges the width of dimples. It has remained recognised that the superior dimples exhibition improved malleability of metal underneath the identical fracture circumstances. In calculation, the descending period and rip edges characterise a greater plastic distortion before the disagreement of specimens, which is unintended indication of plasticity improvement for water jet peening specimens. The untried consequences declared above undoubtedly discovered that the water jet peening development can principally augment the plasticity of AA7075-T6.

IV. Conclusion

This study was conducted using water jet peening as energy on high sequence fatigue behavior of AA7075-T6 samples. The mechanical properties on residual stress, micro hardness, fatigue test and fracture surface morphology of an AA7075-T6 with a thickness of 2 mm were investigated on without and with water jet peening energies of 15 MPa, 20 MPa, and 25 MPa.The results indicated that the RCS can be inducted into the surface of the specimen. water jet peening sample with pulse energy of 25 MPa significantly revealed higher influence as among the other specimens. However, it was significantly indicated that clearer differences of 409

seconds of time and also 1456 fatigue cycle all before failure as compared to the sample without water jet peening.

References

[1] B. Salehnasab and E. Poursaeidi, "Mechanism and modeling of fatigue crack initiation and propagation in the directionally solidified CM186 LC blade of a gas turbine engine," *Engineering Fracture Mechanics*, vol. 225, p. 106842, 2020/02/15/ 2020.

[2] D. Bombač, M. Gintalas, G. Kugler, and M. Terčelj, "Thermal fatigue behaviour of Fe-1.7C-11.3Cr-1.9Ni-1.2Mo roller steel in temperature range 500–700 °C," *International Journal of Fatigue*, vol. 121, pp. 98-111, 2019/04/01/ 2019.

[3] B. Salehnasab, J. Marzbanrad, and E. Poursaeidi, "Transient thermal fatigue crack propagation prediction in a gas turbine component," *Engineering Failure Analysis*, vol. 130, p. 105781, 2021/12/01/ 2021.

[4] E. Maleki, S. Bagherifard, M. Bandini, and M. Guagliano, "Surface post-treatments for metal additive manufacturing: Progress, challenges, and opportunities," *Additive Manufacturing*, vol. 37, p. 101619, 2021/01/01/ 2021.

[5] H. Mahdi, M. Hardisty, K. Fullerton, K. Vachhani, D. Nam, and C. Whyne, "Open-source pipeline for automatic segmentation and microstructural analysis of murine knee subchondral bone," *Bone*, vol. 167, p. 116616, 2023/02/01/ 2023.

[6] L. Wu, K. Zhang, Z. Zhou, G. Wang, and X. Zhang, "Two-step post treatment to improve corrosion resistance and friction performance of Fe-based metallic glasses/crystalline dual-phase coatings," *Journal of Non-Crystalline Solids*, vol. 609, p. 122268, 2023/06/01/ 2023.

[7] B. Salehnasab, J. Marzbanrad, and E. Poursaeidi, "Conventional shot peening treatment effects on thermal fatigue crack growth and failure mechanisms of a solid solution alloy," *Engineering Failure Analysis*, vol. 155, p. 107740, 2024/01/01/ 2024.

[8] H. Soyama, C. Kuji, and Y. Liao, "Comparison of the effects of submerged laser peening, cavitation peening and shot peening on the improvement of the fatigue strength of magnesium alloy AZ31," *Journal of Magnesium and Alloys*, vol. 11, pp. 1592-1607, 2023/05/01/ 2023.

[9] P. Siahpour, M. Y. Amegadzie, A. Tieu, I. W. Donaldson, and K. P. Plucknett, "Ultrasonic pulsed waterjet peening of commercially-pure titanium," *Surface and Coatings Technology*, vol. 472, p. 129953, 2023/11/15/ 2023.

[10] C. K. Yong, E. M. Keating, D. J. Hughes, T. Connolley, G. West, C. C. Wong, *et al.*, "Assessment of residual strain in laser shock peened additive manufactured Inconel 718 using synchrotron X-ray diffraction," *Materialia*, vol. 30, p. 101843, 2023/08/01/ 2023.

[11] M. Ashok Kamde, Y. Mahton, A. Kushwaha, A. Basu, and P. Saha, "Effect of ultrasonic shot peening and intermediate cerium salt conversion bath treatment controlling corrosion of Mg-Y-Zn-based alloy in salt water," *Applied Surface Science*, vol. 648, p. 159094, 2024/03/01/ 2024.

[12] C. Si, W. Sun, Y. Tian, and J. Cai, "Cavitation erosion resistance enhancement of the surface modified 2024T351 Al alloy by ultrasonic shot peening," *Surface and Coatings Technology*, vol. 452, p. 129122, 2023/01/15/ 2023.

[13] H. Li, J. Zhang, L. Hu, and K. Su, "Notch fatigue life prediction of micro-shot peened 25CrMo4 alloy steel: A comparison between fracture mechanics and machine learning methods," *Engineering Fracture Mechanics*, vol. 277, p. 108992, 2023/01/01/ 2023.

[14] K. Sato, Y. Sugimoto, and S. Ohjimi, "Pressure-wave formation and collapses of cavitation clouds impinging on solid wall in a submerged water jet," 2009.

[15] H. Soyama, "Effect of nozzle geometry on a standard cavitation erosion test using a cavitating jet," *Wear*, vol. 297, pp. 895-902, 2013.

[16] M. P. Dhanasekaran, M. Agilan, S. Avinash, K. N. Vidyananda, G. Sudarshan Rao, and D. Roy Mahapatra, "Influence of laser shock peening on Residual stress and microhardness of AA2219 friction stir weld," *Materials Letters*, vol. 356, p. 135586, 2024/02/01/ 2024.

[17] M. Z. Ge, Y. Tang, Y. K. Zhang, and Y. Wang, "Enhancement in fatigue property of Ti-6Al-4V alloy remanufactured by combined laser cladding and laser shock peening processes," *Surface and Coatings Technology*, vol. 444, p. 128671, 2022/08/25/ 2022.

[18] Y. Chen, Q. Wang, H. Roven, M. Karlsen, Y. Yu, M. Liu, *et al.*, "Microstructure evolution in magnesium alloy AZ31 during cyclic extrusion compression," *Journal of Alloys and Compounds*, vol. 462, pp. 192-200, 2008.

[19] A. G. Sanchez, C. You, M. Leering, D. Glaser, D. Furfari, M. E. Fitzpatrick, *et al.*, "Effects of laser shock peening on the mechanisms of fatigue short crack initiation and propagation of AA7075-T651," *International Journal of Fatigue*, vol. 143, p. 106025, 2021/02/01/ 2021.

[20] H. Asgari, J. Szpunar, A. Odeshi, L. Zeng, and E. Olsson, "Effect of grain size on high strain rate deformation of rolled Mg–4Y–3RE alloy in compression," *Materials Science and Engineering: A*, vol. 633, pp. 92-102, 2015.

[21] E. Maawad, Y. Sano, L. Wagner, H.-G. Brokmeier, and C. Genzel, "Investigation of laser shock peening effects on residual stress state and fatigue performance of titanium alloys," *Materials Science and Engineering: A*, vol. 536, pp. 82-91, 2012.